IAC-24,A3,IP,16,x87312

Actuator Blockage Detection in Milli-G

Juliane Skibbe[a]*, Anna Merk[a], Roman Holderried[b]

[a] *Institute of System Dynamics and Control, German Aerospace Center (DLR), Münchener Str. 20, 82234 Wessling*
[b] *Institute of Robotics and Mechatronics, German Aerospace Center (DLR), Münchener Str. 20, 82234 Wessling*
* Corresponding Author *juliane.skibbe@dlr.de*

Abstract

Exploration rover like IDEFIX, the rover of the Martian Moons Exploration Mission (MMX), even when designed with extraordinary diligence, can get stuck in their environment or be affected by other faults. Ground loops for fault detection and isolation are time consuming, especially in a time-limited mission like that of the MMX rover. Thus, on-board fault detection, isolation and recovery (FDIR) in case a rover gets blocked with their actuators is very advantageous. The MMX rover is provided with four identical shoulder modules including a leg and a wheel with one motor each. The available position, torque and current sensors shall be used to detect a blockage and classify if it is positioned at a leg or a wheel to induce the corresponding recovery strategy. To analyze this problem, tests on flight-like hardware were conducted, whereby blockages were induced at different locations at the leg and wheel. In a first analysis, it was observed that only current and torque signals can be used to detect a blockage, but none of the signals can be used alone to isolate a blockage. With the gathered data, logistic regression was used to classify the blockage location in almost all cases correctly. With this result, blockages can be detected on-board and recovered in a further step, which increases the autonomy and hence the reliability of the MMX rover locomotion.
Keywords: Fault detection, fault isolation, actuator blockage

Acronyms/Abbreviations

Clockwise (CW), Counter-clockwise (CCW), Deutsches Zentrum für Luft- und Raumfahrt (DLR, German Aerospace Center), Electronic Box (E-Box), Fault detection, isolation and recovery (FDIR), Locomotion Subsystem (LSS), Martian Moons eXploration (MMX), Robotics and Mechatronics Center (RMC).

1. Introduction

The rover IDEFIX, see Fig. 1, which is part of JAXAs Martian-Moons-eXploration (MMX) mission and jointly developed by the German Aerospace Center (DLR) and Centre National d'Études Spatiales (CNES), is scheduled to touch ground on the Martian moon Phobos in late 2028 or early 2029. Aside from demonstrating wheeled locomotion and autonomous navigation in milligravity for the first time, the main mission goals are to analyze the surface of Phobos using its scientific instruments, such as a thermal mapper (miniRAD) and a Raman Spectrometer (RAX).

The LSS, IDEFIX's Locomotion Subsystem, is capable of not only moving the rover across the surface of Phobos, but also to adjust its pose to fulfil scientific tasks and those necessary to keep the rover alive [1]. It was developed at DLR's Robotics and Mechatronics Center (RMC) and consists of external hardware and an electronic box (E-Box), which is used for data acquisition and control and is integrated into the chassis, as well as the LSS software running on the on-board computer.

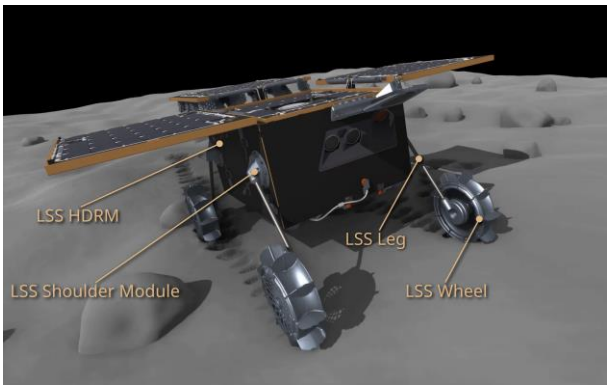

Fig. 1. The IDEFIX rover.

The external components of the LSS consist of four wheels, each mounted on a leg that can be rotated around the joint axis of the shoulder module, as well as the hold-down and release mechanisms (HDRMs) that are fixing the legs until the landing on Phobos has been completed. The main advantages of this configuration include its ability to adapt the rovers wheeled movements to different surface conditions by controlling the ground clearance and the tilt of the chassis. The system design of the LSS and its testing is described in [2] in more detail.

In its operational phase on Phobos, IDEFIX has to withstand harsh environmental conditions. The extreme temperature range, the almost unknown surface conditions on Phobos and the high radiation levels in space environments increase the risks of hardware failure substantially. As it is in contact with the surface,

the LSS is in particular danger of getting damaged, since it could get blocked by rocks and regolith parts or get stuck within the environment.

There are several scenarios where the mission success could be at risk if actuator blockages cannot be resolved either by the rover autonomously or by human decisions within a ground loop. For example, after the landing on Phobos, IDEFIX needs to upright itself so that the solar arrays can be deployed and the battery recharged. Since ground communication is not possible while the solar arrays are folded up, it must be able to take countermeasures against eventual blockages autonomously. Also, throughout the mission, the rover must adjust its pose regularly to align the solar cells towards the sun. Due to the limited battery power, the decision on the action to take in case of a blockage is time critical. A ground loop for determining the next steps based on sensor data will take too much time and is therefore fatal for the rover.

2. Problem formulation

To mitigate the risks to the mission, algorithms that are able to reliably detect and locate blockages of the IDEFIX actuators are advantageous. They are to be embedded into the Fault Detection, Isolation and Recovery (FDIR) module of the LSS software [3].

2.2 Fault detection and isolation

To increase the autonomy on-board of the rover, the sensor data needs to be used for fault detection and fault isolation. Fault detection means, that an anomaly is detected, where fault isolation identifies where this anomaly is located and how severe it is. After these two steps, a recovery strategy can be applied to avoid a failure and with it an incapacity of the rover's locomotion system. In case of an actuator blockage, two different recovery strategies are conceivable: In case of a motor blockage, an internal stuck recovery strategy can be activated to loosen a clamped motor. This can be repeated until the deadlock is released. The second kind of blockage is an external blockage, for example if the grousers of the wheel clamp between two stones. Depending on factors like mission phase, localization of the blockage and others, a different recovery strategy might be chosen. In a severe fault case, the present movement needs to be stopped and the rover needs to continue operating in safe mode. This avoids dangerous actions until a command from ground control releases the rover from this blockade situation.

To know which recovery strategy needs to be performed, the blockage fault must be detected and then isolated in the sense of localized. Hence, the aim of this study is to develop a law for the detection and isolation of a blockage fault in the MMX leg hardware. The distinction of the blockage position shall be formed by the available sensor data. The present sensors in the legs are a motor current sensor, a relative position sensor in the motor, an absolute position sensor in the joint and a torque sensor. The wheels have a motor current sensor and the relative positions sensor. This leads to six sensors in total for each leg-wheel-pair.

2.1 Sensor data

The analysis is based on an extensive amount of sensor data provided by the test hardware. The most relevant data sources for the design of a blockage detecting FDIR algorithm are listed below.

Torque sensors

The torque sensors are located at the joint of each shoulder module. They provide direct measurements of the torque that is needed to actuate the leg. Hence, a leg blockage can be directly seen in this data. A certain amount of hysteresis must be considered when converting the raw values of the sensor into its SI values, depending on how the direction of movement has been changed before the sample was taken. This characteristic qualifies the torque sensor values to be rather used for relative measurement when monitoring an actuator movement.

Motor current measurements

The motor current is directly proportional to the torque that the motor applies to drive the output shaft. Hence, it could also be used to detect blockages of the actuators. Due to the low gravity on Phobos [4], the actuation of the LSS needs to be very slow to prevent uncontrolled movements of the rover. The drives were therefore designed with three gear stages and a combined ratio of approximately 2225:1. One stage consists of a strain wave gear that introduces a significant friction torque to the motor by itself, which is also not constant within one revolution. Even worse, the friction torque also has a strong temperature dependence due to the lubrication. A blockage detection based solely on the motor current will therefore not be feasible. For further readings, refer to [5].

Positional measurements

Each motor module of the rover integrates a Hall effect sensor, which is used for motor commutation and relative position measurement. Additionally, each shoulder module joint is equipped with a potentiometer measuring the absolute angle of the joint within one mechanical revolution. A small angular dead zone must be considered when converting the raw potentiometer values into its SI representatives. Both positional measurements can be used by an algorithm to improve the reliability of the blockage detection

The detection of a fault is based on unexpected variation of the sensor values. Within this work, it is

studied if a constant threshold that needs to be exceeded is sufficient to detect a fault or if the threshold depends on additional parameters. It will be shown that for the isolation, the different sensor values need to be compared and their combination has to be considered.

3. State of the Art

Traditional fault detection and isolation methods often rely on model-based approaches that use system models to detect deviations that indicate a fault. Castillo et al. [6] discuss how these methods are valuable for systems operating in non-linear environments, where complex interactions between components can lead to unexpected behaviors. However, the main limitation of these model-based approaches lies in their dependence on the precision and availability of the system's dynamic models.

To overcome these restraints of model-based methods, the literature shows a shift towards approaches that do not rely solely on precise models. Residual generation and parameter estimation techniques have gained an increasing amount of interest for their effectiveness in real-time fault detection [7,8]. Recent research on aerospace systems [9] has furthermore shown that generating residuals by comparing system outputs with expected values can effectively detect anomalies in real-time conditions. This represents a crucial capability for space missions, where delays in fault detection can lead to mission failure.

Additionally, sliding mode observers have been presented as a robust solution for FDI in systems with high uncertainty, such as those operating in milligravity environments. Zhu et al. [10] highlight the robustness of sliding mode observers in managing such system uncertainties.

Traditional fixed threshold methods face challenges in environments with high uncertainty, like those encountered by the MMX rover. Here, effects such as wheel-soil interaction on uneven terrain can cause unexpected slips or loss of traction. Curry et al. [11] point out that fixed thresholds can result in false positives or missed detections, especially in systems where two actuators interact in unpredictable ways. Therefore, while this method is regularly used to detect faults in the industry [12,13,14], it is often insufficient when dealing with isolating complex fault scenarios such as an actuator blockage in a locomotion system. In these cases, the sensor data requires a more nuanced interpretation to determine the location of the fault.

In response to these challenges, there has been an increasing emphasis on data-driven approaches, particularly statistical methods like logistic regression [15,16]. Logistic regression offers a flexible and powerful way of mapping sensor data to fault scenarios by capturing the interdependencies among sensor readings [17]. This approach shows potential to be effective in robotics and aerospace applications for improving fault isolation accuracy, thus allowing for an appropriate recovery strategy to be initiated.

While many of the mentioned technical systems in literature are similar in their conditions and objectives to the FDI system of the MMX rover, they also differ in some regards. Firstly, the fault cases to be detected in the given literature are known and small in numbers. In the context of this study, only the specific fault cases of a wheel joint actuator and leg joint actuator blockage must be detected and distinguished from each other as well as from the nominal operational state. In the context of this limitation and in view of the restrictions of computational power and space on the rover itself, the use of simple approaches is favored.

4. Test

To explore how sensor values might vary under different conditions, experiments on the MMX locomotion unit were conducted using a customized testbench at the DLR-RMC as shown in Fig. 2. The following sections present the setup, the results and their interpretation.

4.1 Setup

The testbench was designed to replicate the operating environment of the rover's locomotion unit and to assess the effectiveness of fault detection strategies on the collected data. The setup involved a side panel of the rover chassis mounted on an interface frame, with a single leg-wheel-pair attached. This leg-wheel-pair has a total weight of 0.488 kg and is equipped with two independent motors, one for the leg and one for the wheel. To minimize the impact of Earth's gravity and get closer to the microgravity environment of Phobos, the testbench was set up horizontally.

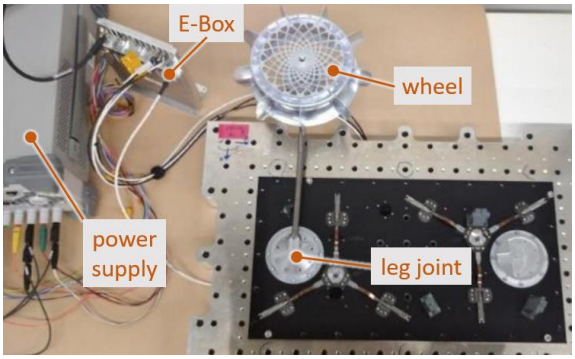

Fig. 2: Test bench set up: Power supply and motor controller on the left, MMX leg and wheel in the centre.

The E-Box connected to this setup served as the interface between the software controlling the rover and its mechanical components, more precisely the motors and sensors. This E-Box was linked to a computer via a

SpaceWire-to-USB connection, executing the commands and retrieving the data. In the flight hardware, the E-Box will be connected via SpaceWire to the on-board computer. The test setup simultaneously recorded multiple measurements, including the current in the two motors, data from Hall effect sensors within the motors, readings from a potentiometer, and the torque value at the leg joint, with a frequency of 17 Hz. This is even faster than in the MMX mission, where the software will receive the data with a frequency of 10 Hz. All sensor values are measured with 40 kHz in the Firmware in the E-Box.

For the motor currents and the torque data, the mean, minimum and maximum values are sent from the E-Box to the software. For the absolute and relative positions, the latest value when reading from SpaceWire is provided to the software. An overview over the data rates is given in Table 1.

Table 1. Sensor measurement rates for blockage detection in the LSS of IDEFIX.

Sensor value	Measurement rate		
	In E-Box firmware	In test software	In mission software
Torque	40 kHz	Mean/max/ min in 17 Hz	Mean/max/ min in 10 Hz
Current	40 kHz	Mean/max/ min in 17 Hz	Mean/max/ min in 10 Hz
Potentiometer	40 kHz	Last position 17 Hz	Last position 10 Hz
Hall effect	40 kHz	Last position 17 Hz	Last position 10 Hz

To protect the delicate sensors from damage, particularly the torque sensor which designed for low torques (±2 Nm), safety mechanisms were integrated into the testbench. These included an automatic motor shutdown when current thresholds were exceeded, as well as a fail-safe obstacle mechanism, consisting of a torque wrench set to 2 Nm to prevent excessive moments. Therefore, the current will never exceed a certain limit in the test results.

4.2 Execution

The experiments systematically varied several key parameters to understand their impact on sensor measurements. These parameters and their different values are collected in Table 2. The direction of motor rotation was one such parameter, with tests conducted to determine whether clockwise (cw) or counter-clockwise (ccw) rotation influenced current and torque readings, potentially requiring different fault detection thresholds. Another critical parameter was the speed of rotation. Experiments were carried out at four different speeds (0 mrad/s, 10 mrad/s, 30 mrad/s, 50 mrad/s) for the wheel and leg, respectively, to analyze the relationship with current sensor readings and any corresponding effects on torque measurements. These rates are realistic speeds for the mission, since speeds have to kept low due to the low gravity on Phobos.

Table 2. Testing parameters and their variations.

	Variations
Actuator direction	Clockwise, counter-clockwise, none
Actuator speed	0 mrad/s, 10 mrad/s, 30 mrad/s, 50 mrad/s
Blockage position	Leg 9 cm, leg 16 cm, wheel

Inter-motor influences were also examined by operating both motors (leg and wheel) in parallel to detect any voltage drops or increased friction that might affect sensor data. Finally, actuator blockage scenarios were simulated by placing an obstacle at different points along the leg shaft and at a wheel grouser, as depicted in Fig. 3. These tests were essential for defining fault detection and isolation techniques by comparing the fault scenario data with previously measured baseline sensor values. For each configuration, multiple sets of measurements were collected to ensure accuracy and reduce statistical errors. For the evaluation, these data sets were averaged. In total, 120 tests with the blockage at the wheel and 210 tests with a blockage at 9 cm and at 16 cm of the leg, were conducted respectively. Additionally, 288 tests without a blockage for reference were executed.

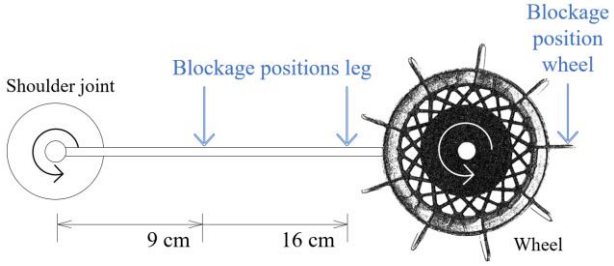

Fig. 3: Experiment setup for obstacle-induced blockages.

4.3 Results

4.3.1 Current at different speeds

First, the influence of motor speeds and motor directions on current measurement in the absence of any blockage was examined. To achieve this, one motor was either left stationary or operated at a constant speed, while the speed of the second motor was rotated at the rates of 10 mrad/s, 30 mrad/s and 50 mrad/s. Additionally, the direction of rotation was altered: clockwise and counter-clockwise, since both moving directions appear during the rover's mission. The results of the observations are presented in Fig. 4 to Fig. 7.

From these data, it is evident that as the speed of the motor increases, there is a corresponding increase in the current drawn. This can be explained by the speed dependency of the friction of the gear: for this reason, the demanded torque increases, which subsequently leads to a higher current consumption.

Additionally, it can be observed that the speed of the second motor does not affect the current consumption of the first motor. This suggests that there are no cross-coupling effects between the motors in regards of the current consumption. With that knowledge, the speed of the second motor can be ignored when interpreting the individual motor current signals.

On top of that, there is no significant difference in the clockwise or counter-clockwise direction, which is expected. From this we can conclude that the direction of rotation of the actuator can be ignored in the subsequent interpretations.

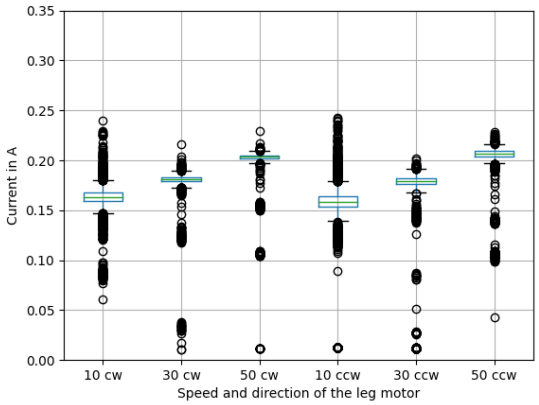

Fig. 4. Current of the leg motor while the wheel motor rotates with a rate of 0 mrad/s.

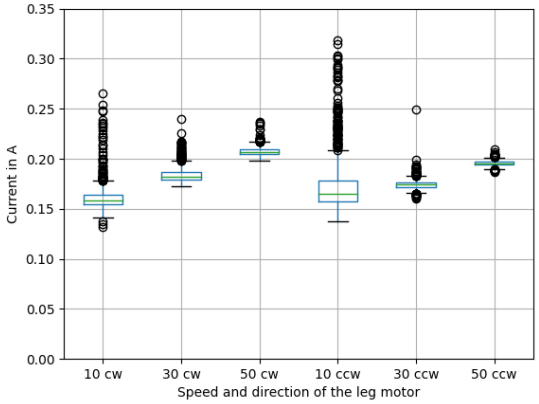

Fig. 5. Current of the leg motor while the wheel motor rotates with a rate of 30 mrad/s.

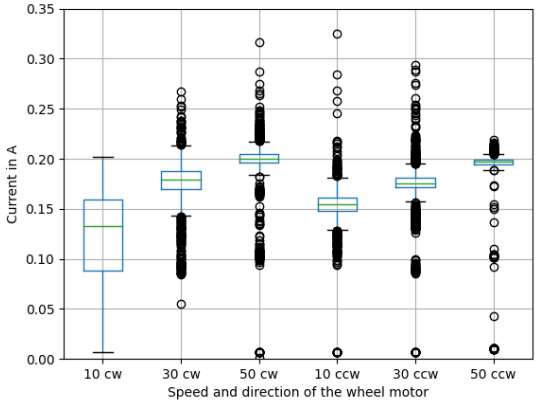

Fig. 6. Current of the wheel motor while the leg motor rotates with a rate of 0 mrad/s.

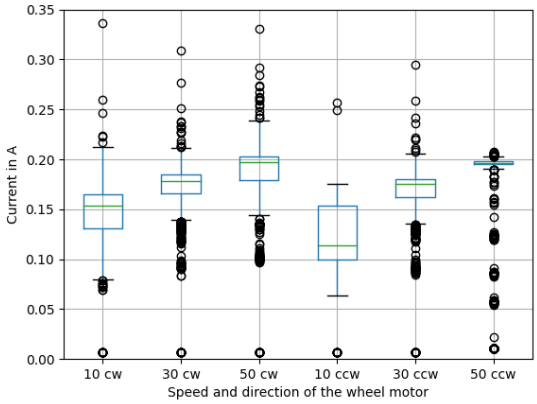

Fig. 7. Current of the wheel motor while the leg motor rotates with a rate of 30 mrad/s.

4.3.2 Signals with blockage

For a comparison of the relevant signals with the different blockage positions, all of the available sensors are considered, see Fig. 8 to Fig. 13. It is distinguished between the three different leg speeds at movement (10 mrad/s, 30 mrad/s, 50 mrad/s) and the three different blockage positions (leg 9 cm, leg 16 cm, wheel), which leads to nine different measurement series. The wheel speed can be neglected, as shown for the current in the previous subsection and also examined for the other sensors in preliminary studies. Since the variation of the leg speeds result in different test durations, the measurement series were linearly interpolated to the highest number of sampling points. This approach allows for better comparability of the results.

For the torque and current values, the mean value of the last period is considered. For the hall and potentiometer data, the latest position when reading the SpaceWire data from the E-Box is used.

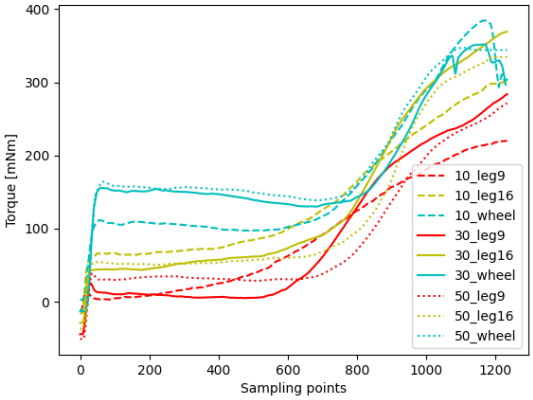

Fig. 8: Torque signals for different leg speeds and blockage positions.

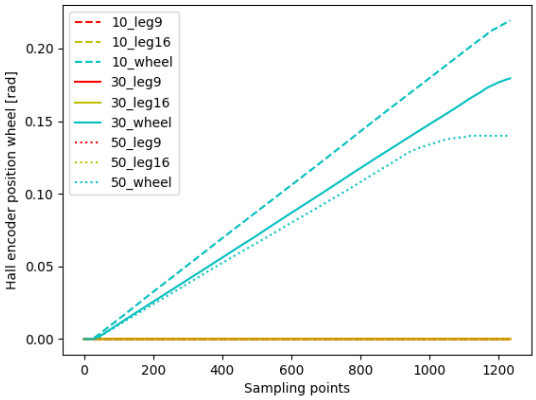

Fig. 11. Hall encoder positions of the wheel for different leg speeds and blockage positions.

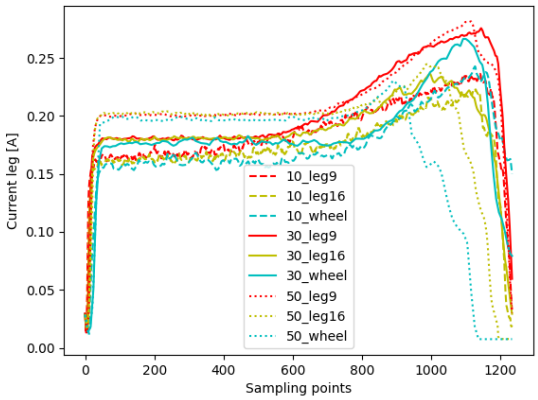

Fig. 9. Motor current of the leg for different leg speeds and blockage positions.

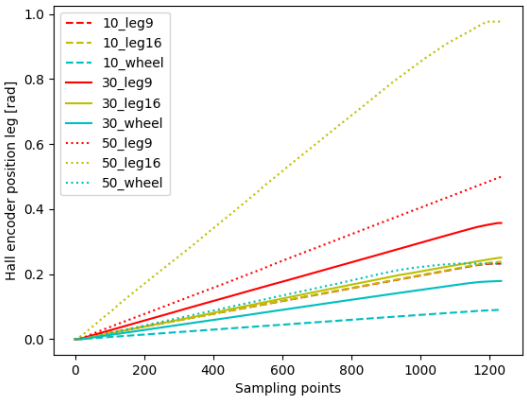

Fig. 12. Hall encoder positions of the leg for different wheel speeds and blockage positions.

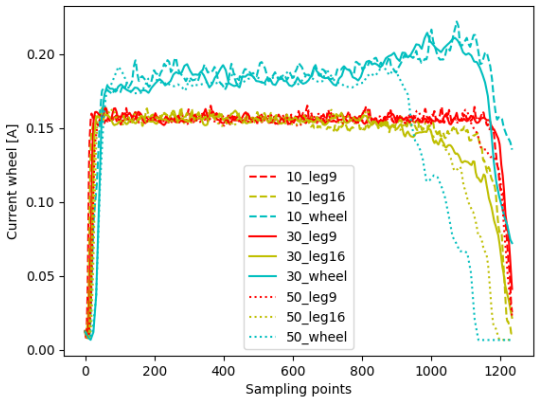

Fig. 10. Motor current of the wheel for different leg speeds and blockage positions.

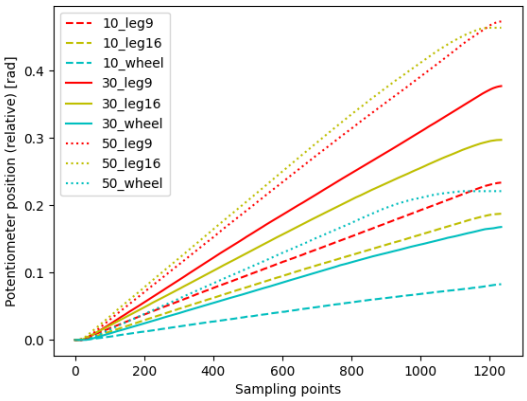

Fig. 13. Potentiometer positions of the leg for different leg speeds and blockage positions.

The torque, see Fig. 8, increases when the leg starts to move. It rises again with the blockage, but a significant difference between the different blockage locations cannot be identified.

The current in the leg motors, as shown in Fig. 9, increases when the leg starts to move, as expected. The value of the current depends on the speed: The higher the motor speed, the higher the current value. When touching the barrier, the current increases until the safety mechanism that was explained in section 4.1 is activated. It must be noted that the mean values are consulted, hence not all plotted maxima reach the same peak height. Here, too, regardless of consideration of the speed, no difference between the different blockage positions is observable. Nevertheless, looking at the current of the wheel motors (Fig. 10), a wheel blockage can be detected compared to a leg blockage: while the current of the wheel is increasing, the current of the leg stays constant within its noise.

The hall encoder signal for the wheel (Fig. 11) do change only for the wheel blockage. For the leg blockage, pure leg movements were considered. The deceleration of the rate is clearly recognizable at the end of each measurement series, where the blockage applies, but it never leads to a total stagnation of the Hall position value. The same behavior can be observed in the position of the leg from the Hall sensor (Fig. 12) and the potentiometer (Fig. 13), both converted to radians. To interpret whether this slowdown is due to an external blockage or due to a lower commanded speed, the data need to be compared to the desired position values.

In Fig. 14 and Fig. 15, the difference between the commanded Hall encoder position and the actual Hall encoder position is shown. This difference is the discrepancy between the actual state and the desired state, which are the inputs for the motor controller. It must be noted that the Hall encoder values are always integers, but the figures show decimals due to the averaging of multiple test runs. For both motors, no significant drift at the end of the measurement series is observable. It can therefore be concluded, that the difference between the desired and the actual Hall encoder position can not be taken into account for a blockage detection at all.

In Table 3 is a summary of this preceding analyzation, which shows if a single sensor signal can be used to detect and isolate a blockage. It is remarkable, that with a single sensor signal, a blockage cannot be located, thus isolated. The pure existence of a blockage can be determined by the torque and current signals. However, the torque and current signals are speed dependent, which implies that a blockage detection threshold requires to be speed dependent as well – otherwise, a blockage would be detected too late for a low speed or there would be a high number of false positives for high speeds.

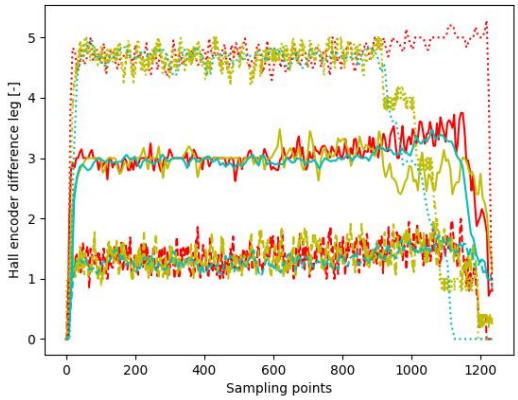

Fig. 14. Difference of commanded and desired Hall encoder position of the leg for different wheel speeds and blockage positions.

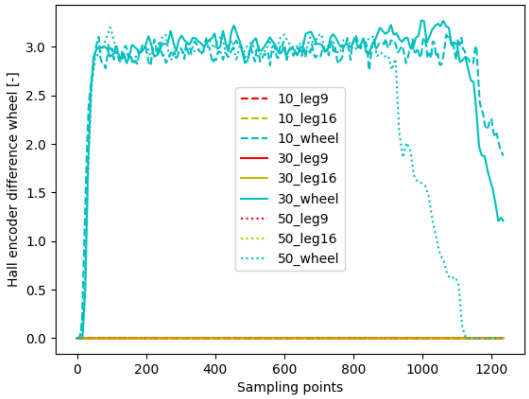

Fig. 15. Difference of commanded and desired Hall encoder position of the wheel for different leg speeds and blockage positions.

Table 3. Summed up if a single sensor signal can be used for blockage detection and isolation.

	Usable for blockage detection	Usable for blockage isolation
Torque	Yes	No
Wheel current	Yes	Partially
Leg current	Yes	No
Potentiometer	No	No
Wheel Hall	No	No
Leg Hall	No	No
Wheel Hall difference	No	No
Leg Hall difference	No	No

4.3.3 Logistic regression for fault isolation

Since the location of a blockage cannot be determined by residuals based on observation of single signals, the combination of the signals has to be considered. Logistic regression is therefore applied here. It is a common method that estimates the probability that data are from a certain class by using a linear combination of these data. By applying a decision threshold, the observations are classified into the most probable class. Within that approach, the test scenarios can be classified based on the measured data.

For all conducted tests, the following values were calculated for the torque, wheel current and leg current sensors: Minimum, maximum, median, mean, variance, standard deviation, skewness and kurtosis. The data are then split into a training set and a test set in the ration 4:1. The training set is for generation of the logistic regression model and the test set is for evaluation via cross-validation.

In a first approach, it was distinguished between the four cases “no blockage”, “blockage at leg 9cm”, “blockage at leg 16 cm” and “blockage at wheel”. The outcome of the classification of the test set is shown in Fig. 16. On the vertical axis, the actual test type is stated and on the horizontal line, the classification resulting from the logistic regression is given. On the main diagonal, the number of true positives can be read. In total, the rate of correctly classified tests is 89,8%. This number has potential for optimization, since a wrong classification leads to an improper chosen fault recovery strategy, which is undesirable.

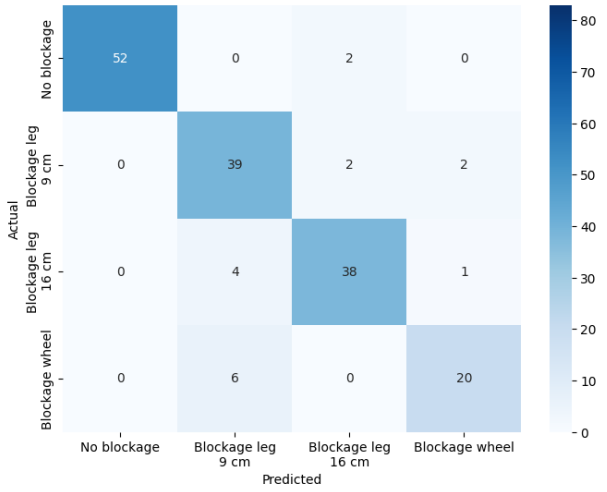

Fig. 16. Confusion matrix for classification of no blockage, leg blockage at 9cm, leg blockage at 16cm and wheel blockage.

As the exact blockage position at the leg is less relevant for the selection of the recovery algorithm, the test cases “blockage at leg 9 cm” and “blockage at leg 16 cm” were merged to a single class “blockage at leg”. The splitting of the test cases into training data and test data was repeated and a new logistic regression model was generated. The result is shown in Fig. 17. The new rate of correctly classified tests is now at 95,2%, which is a good improvement. It must be noted that the absolute number of true-positive cases for the “no blockage” and “blockage at wheel” differ slightly from the first approach because of the regeneration of the model.

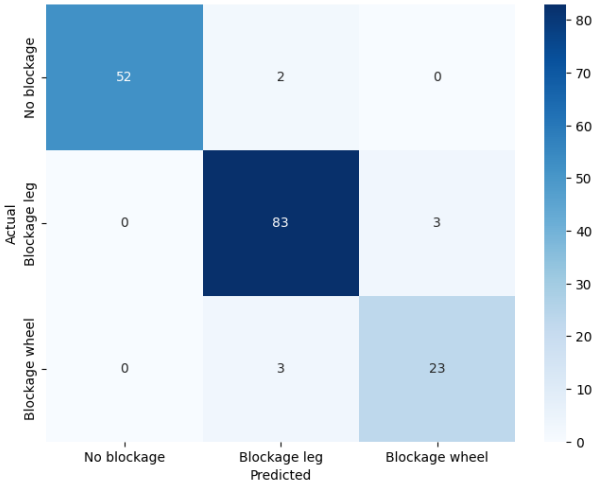

Fig. 17. Refined confusion matrix for classification of no blockage, leg blockage and wheel blockage.

5. Discussion and future work

Only specific scenarios were selected for analysis in this study and several potential cases were not included. Additional blockages at various positions on the wheel should be investigated to get a more comprehensive understanding. Scenarios such as combinations of leg and wheel blockages, areal blockages like being embedded in sand, and internal motor blockages were not considered. Moreover, driving on different terrain with varying slopes can have a substantial impact on sensor measurements. The interaction between these surfaces and the rover's wheels, particularly under different inclines, might produce sensor readings that differ considerably from those observed in the selected scenarios. Additionally, it is likely that sudden blockages as they were investigated in this study, would produce distinct sensor patterns compared to scenarios where an object like a stone moves along with the wheel. All these scenarios could have significant implications for the system's behavior and require further exploration.

However, testing these scenarios on physical hardware presents challenges. The behavior of the rover under Earth's gravity differs from its behavior under the gravity of Phobos. This difference complicates the replication of realistic conditions for certain blockages, limiting the applicability of tests on hardware under Earth gravity. To address these limitations, the physical

simulation of the rover [18] can be used, allowing for the evaluation of these scenarios under more accurate gravitational conditions.

6. Conclusion

The detection of a leg or wheel blockage could be identified successfully by observation of the torque and current sensor data. However, the positions of a blockage at an IDEFIX leg could not be determined by observing individual sensor signals alone. To achieve this, it was necessary to analyze the combination of multiple signals. With a large set of measurements from the test hardware in specific fault scenarios, combined with logistic regression, it is possible to accurately classify the blockage locations in nearly all cases.

References

[1] H.-J. Sedlmayr, S. Barthelmes, R. Bayer, et. al.: MMX - Development of a Rover Locomotion System for Phobos. 2020 IEEE Aerospace Conference, Big Sky, MT, USA, 2020.

[2] V. Langofer, R. Bayer, A. Kolb and K. Sasaki: MMX Locomotion Subsystem: mechanics for extraterrestrial low gravity drive. 2023 IEEE Aerospace Conference, Big Sky, MT, USA, 2023.

[3] J. Skibbe, E. Aitier, S. Barthelmes et al.: Fault Detection, Isolation and Recovery in the MMX Rover Locomotion Subsystem. 2023 IEEE Aerospace Conference, Big Sky, MT, USA, 2023.

[4] J. Bertrand, S. Tardivel, F. IJpelaan et al.: Roving on Phobos: Challenges of the MMX Rover for Space Robotics. Proceedings of 15th Symposium on Advanced Space Technologies in Robotics and Automation. 15th Symposium on Advanced Space Technologies in Robotics and Automation, 2019-05-27 - 2019-05-28, Noordwijk, Netherlands.

[5] S. Barthelmes, S., Buse, F., Chalon, M. et al.: Characterization of the MMX Rover Locomotion Flight Model for Check-Out and Parameterization. 2024 IEEE Aerospace Conference, Big Sky, MT, USA, 2024.

[6] I. Castillo, T. F. Edgar, and R. Dunia: Nonlinear Detection and Isolation of Multiple Faults Using Residuals Modeling. Industrial & Engineering Chemistry Research, vol. 53, no. 13, pp. 5217–5233, Apr. 2014.

[7] J. Luo, M. Namburu, K. R. Pattipati, L. Qiao, and S. Chigusa: Integrated Model-Based and Data-Driven Diagnosis of Automotive Antilock Braking Systems. IEEE Transactions on Systems, Man, and Cybernetics - Part A: Systems and Humans, vol. 40, no. 2, pp. 321–336, Mar. 2010.

[8] W. Ziling, X. Aiqiang, and Y. Zhiyong: Application of Model-based and Data-driven Techniques in Fault Diagnosis. 2007 8th International Conference on Electronic Measurement and Instruments, Xian, China: IEEE, Aug. 2007, pp. 3-451-3–454.

[9] D. Asadi: Actuator Fault Detection, Identification, and Control of a Multirotor Air Vehicle Using Residual Generation and Parameter Estimation Approaches. International Journal of Aeronautical and Space Sciences, vol. 25, no. 1, pp. 176–189, Jan. 2024.

[10] F. Zhu, Y. Shan, and Y. Tang: Actuator and Sensor Fault Detection and Isolation for Uncertain Switched Nonlinear System Based on Sliding Mode Observers. International Journal of Control, Automation and Systems, vol. 19, no. 9, pp. 3075–3086, Sep. 2021.

[11] T. Curry, E. G. Collins, and M. Selekwa: Robust fault detection using robust l/sub 1/ estimation and fuzzy logic. Proceedings of the 2001 American Control Conference. Arlington, Virginia, USA: IEEE, 2001, pp. 1753–1758 vol.2.

[12] J. Stoustrup, H. Niemann, and A. La Cour-Harbo: Optimal threshold functions for fault detection and isolation. Proceedings of the 2003 American Control Conference, 2003. Denver, Colorado, USA. IEEE. pp. 1782–1787.

[13] A. Emami-Naeini, M. M. Akhter, and S. M. Rock: Effect of model uncertainty on failure detection: the threshold selector. IEEE Transactions on Automatic Control, vol. 33, no. 12, pp. 1106–1115, Dec. 1988.

[14] K. Le, Z. Huang, C. W. Moon, and A. Tzes: Adaptive thresholding-a robust fault detection approach. Proceedings of the 36th IEEE Conference on Decision and Control, San Diego, California, USA: IEEE, 1997, pp. 4490–4495.

[15] T. Kerdsiri and R. Gullayanon: Early Fault Detection based on Ball Bearing Vibration Analysis using Multinomial Logistic Regression. Proceedings of the 2017 International Conference on Intelligent Systems, Metaheuristics & Swarm Intelligence, Hong Kong: ACM, Mar. 2017, pp. 152–156.

[16] İ. Kabasakal, F. D. Keskin, A. Koçak, and H. Soyuer. A Prediction Model for Fault Detection in Molding Process Based on Logistic Regression Technique. Proceedings of the International Symposium for Production Research 2019, N. M. Durakbasa and M. G. Gençyılmaz, Eds., in Lecture Notes in Mechanical Engineering. Springer, Cham. 2020, pp. 351–360.

[17] M. P. LaValley: Logistic regression. Circulation, vol. 117, no. 18, pp. 2395–2399, May 2008.

[18] F. Buse, A. Pignède, J. Bertrand, S. Goulet and S. Lagabarre: MMX Rover Simulation - Robotic Simulations for Phobos Operations. 2022 IEEE Aerospace Conference (AERO). Big Sky, MT, USA, 2022.